Applied Surface Science 338 (2015) 146–153

Contents lists available at ScienceDirect

Applied Surface Science

journal homepage: www.elsevier.com/locate/apsusc

Effect of TiO_2, ZrO_2, and TiO_2–ZrO_2 on the performance of CuO–ZnO catalyst for CO_2 hydrogenation to methanol

Jie Xiao, Dongsen Mao*, Xiaoming Guo, Jun Yu

Research Institute of Applied Catalysis, School of Chemical and Environmental Engineering, Shanghai Institute of Technology, Shanghai 201418, PR China

ARTICLE INFO

Article history:
Received 20 September 2014
Received in revised form 25 January 2015
Accepted 18 February 2015
Available online 24 February 2015

Keywords:
CuO–ZnO catalyst
TiO_2
ZrO_2
CO_2 hydrogenation
Methanol synthesis

ABSTRACT

The influence of TiO_2, ZrO_2, and TiO_2–ZrO_2 mixed oxide on the catalytic performance of CuO–ZnO catalyst in the methanol synthesis from CO_2 hydrogenation was studied. The catalysts were prepared by oxalate co-precipitation method and characterized by TGA, N_2 adsorption, XRD, reactive N_2O adsorption, XPS, H_2-TPR, H_2-TPD, and CO_2-TPD techniques. Characterization results reveal that all the additives improve the CuO dispersion in the catalyst body and increase the Cu surface area and adsorption capacities of CO_2 and H_2. The results of catalytic test reveal that the additives increase both the CO_2 conversion and methanol selectivity, and TiO_2–ZrO_2 mixed oxide is more effective than single components of TiO_2 or ZrO_2. Moreover, the activity of methanol synthesis is correlated directly with CO_2 adsorption capacity over the catalysts.

1. Introduction

Recently, global warming caused by the increase in the CO_2 concentration in the atmosphere and the depletion of fossil fuels has received great attention by many researchers [1]. Catalytic conversion of CO_2 to liquid fuels or other valuable chemicals has a positive impact on these important environmental and energy issues [2,3]. Up to now, most of the existing research focuses on CO_2 hydrogenation to methanol, because methanol is an important feedstock for the organic chemical industry and a potential alternative to fossil fuels [4,5]. Furthermore, the convenient manufacture of H_2 on large scales from renewable sources including solar energy, hydropower, and biomass also supports the new process [6].

Currently, methanol is produced at industrial scale by feeding syngas ($CO + H_2$) containing minor amount (<5%) of CO_2 on Cu–ZnO/Al_2O_3 catalysts operating at 493–573 K and 5–10 MPa [7]. The Cu–ZnO/Al_2O_3 catalysts have a considerably high activity for methanol synthesis from syngas. However, their unsatisfactory CO_2 hydrogenation performance, due to a negative effect of water in the presence of the hydrophilic alumina carrier [7,8], is pressing the discovery of alternative catalyst formulations including copper as activity phase and various oxide supports and promoters like ZnO [9], Al_2O_3 [10,11], TiO_2 [11–15], SiO_2 [11,15], ZrO_2 [15–19], CeO_2 [20,21], or their combinations [20–22]. Among the additives studied, ZnO, ZrO_2, and TiO_2 are very promising catalyst supports and/or promoters. The promoting effect of ZnO on copper can create a unique site at the Cu/ZnO interface and change in the heat of adsorption of reactants [9]. The addition of ZrO_2 could enhance the copper dispersion [16] and the surface basicity [23], which in turn improves the catalytic activity and the adsorption of CO_2 [24]. Tagawa et al. [13] investigated the effects of acidity and basicity of support on performance of Cu-based catalysts and found that amphoteric supports (Al_2O_3, TiO_2, ZrO_2) showed high activities. Among them, TiO_2 support can suppress effectively the reverse water gas shift reaction, hence showing the highest methanol selectivity [25]. On the other hand, Bando et al. [11] reported that the Cu/TiO_2 catalyst showed the highest turnover frequency (TOF) among three catalysts (Cu/Al_2O_3, Cu/SiO_2, and Cu/TiO_2). In a word, certain promoters could generate a synergistic effect on the active components, modulate the active sites, prevent the formation of spinel and enhance the adsorption of intermediate species, etc. However, the quaternary CuO–ZnO–TiO_2–ZrO_2 catalyst has been little reported to date [26].

In this paper, CuO–ZnO catalysts promoted with TiO_2, ZrO_2, or TiO_2–ZrO_2 mixed oxide were prepared by an oxalate co-precipitation method and tested for the methanol synthesis from CO_2 hydrogenation, aiming to improve the catalytic performance of CuO–ZnO catalysts. The physicochemical properties of the prepared catalysts were characterized extensively by TGA, N_2 adsorption, XRD, reactive N_2O adsorption, XPS, H_2-TPR, H_2-TPD, and CO_2-TPD

* Corresponding author. Tel.: +86 21 6087 3625; fax: +86 21 6087 3625.
E-mail address: dsmao@sit.edu.cn (D. Mao).

http://dx.doi.org/10.1016/j.apsusc.2015.02.122
0169-4332/

techniques. Furthermore, the catalytic performances of the catalysts were discussed in relation to the results of physicochemical characterizations.

2. Experimental

2.1. Catalyst preparation

The catalysts were prepared by an oxalate co-precipitation method with the proportion of CuO/ZnO/M = 40/40/20 (M represents TiO_2, ZrO_2, or TiO_2–ZrO_2 with TiO_2/ZrO_2 = 10/10, molar ratio). Firstly, the required amounts of metal nitrates/metal oxide ($Cu(NO_3)_2{\cdot}3H_2O$, $Zn(NO_3)_2{\cdot}6H_2O$, TiO_2, and $Zr(NO_3)_4{\cdot}5H_2O$) were added in deionized water to form a solution or a suspension and then the oxalic acid ($H_2C_2O_4{\cdot}2H_2O$) solution (0.8 M) was dropped into the above solution or suspension under constant stirring at room temperature for 0.5 h. The molar ratio of the oxalic acid to the total metal ions was 1.2:1 to ensure all metal ions to be precipitated. The precipitates were kept in an ultrasound bath operating at 47 kHz with a power of 30 W for 1 h. Afterwards, the precipitates were aged at 363 K for 3 h, and then filtered, thoroughly washed with 343 K hot deionized water, and dried at 383 K overnight. Dried samples were ground to fine powders and were calcined by ramping at 2 K min^{-1} to 673 K for 4 h in air. Hereafter, the CuO–ZnO (CuO/ZnO = 50/50, molar ratio), CuO–ZnO–TiO_2, CuO–ZnO–ZrO_2, and CuO–ZnO–TiO_2–ZrO_2 catalysts are denoted as CZ, CZT, CZZ, and CZTZ, respectively.

2.2. Catalyst characterization

Thermogravimetric analysis (TGA) was carried out on a thermal analyzer (STA 499 F3, NETZSCH) at a heating rate of 10 K min^{-1} under a continuous flow of air (50 mL min^{-1}).

Full nitrogen adsorption/desorption isotherms at 77 K were obtained after outgassing the sample under vacuum at 473 K for 10 h, using a Micromeritics ASAP2020 M + C adsorption apparatus. The BET specific surface area (S_{BET}) was calculated using a value of 0.162 nm^2 for the cross-sectional area of the nitrogen molecule. Pore size distributions were determined by the BJH method using the equation of Halsey.

X-ray diffraction (XRD) patterns were recorded with a PANalytical X'Pert diffractometer operating with Ni β-filtered Cu Kα radiation at 40 kV and 40 mA. Two theta angles ranged from 10° to 70° with a speed of 6° min^{-1}.

Cu and Zn contents of the calcined catalysts were determined by atomic absorption spectroscopy (AAS) on acid-digested samples, using a SpectrAA-220 atomic absorption spectrometer (VARIAN).

The metallic copper surface area (S_{Cu}) in the reduced catalyst was determined using a N_2O chemisorption method [18]. Once the catalyst was reduced in a 10% H_2/N_2 mixture at 573 K for 1 h, it was exposed to a flow of He and cooled to the chemisorption temperature (333 K). Then, a flow of 2 vol% N_2O/He gas mixture was fed into the reactor. The N_2 produced by the decomposition of N_2O on the exposed Cu atoms was detected using a mass spectrometer (Pefeiffer Vacuum Quadstar, 32-bit). The metallic copper surface density of 1.46×10^{19} Cu atoms/m^2 and a molar stoichiometry of N_2O/Cu = 0.5 were used to calculate the S_{Cu} [7].

X-ray photoelectron spectroscopy (XPS) measurements were performed on a Kratos Axis Ultra DLD spectrometer equipped with an Al Kα (1486.6 eV) X-ray exciting source. The pass energy of the analyzer was set at 40 eV. The banding energies were referenced to the adventitious C 1s peak at 284.6 eV (accuracy within ±0.3 eV).

Hydrogen temperature-programmed reduction (H_2-TPR) measurements were performed in a continuous flow apparatus fed with a 10% H_2/N_2 mixture flowing at 30 mL min^{-1} and heated at a rate of 5 K min^{-1} to 573 K. A ca. 0.1 g catalyst sample was used, with H_2 consumption monitored by a thermal conductivity detector (TCD).

Hydrogen temperature-programmed desorption (H_2-TPD) was carried out in a quartz tubular reactor. Firstly, the catalyst sample was reduced at 573 K for 1 h in a flow of 10% H_2/N_2 mixture. Then the sample was cooled to 323 K and further saturated in H_2/N_2 mixture for 0.5 h, followed by flushing in N_2 for 1 h. The TPD measurements were conducted in a N_2 stream (30 mL min^{-1}) from 323 to 773 K at a heating rate of 5 K min^{-1}. The change of hydrogen signal was monitored by a TCD.

The basicity of the catalyst was measured by CO_2 temperature-programmed desorption (CO_2-TPD). Prior to the adsorption of CO_2, the catalysts were reduced at 573 K for 1 h in a flow of 10% H_2/N_2 mixture. Then the sample was cooled to 323 K and further saturated in 10% CO_2/N_2 (30 mL min^{-1}) mixture for 0.5 h, followed by flushing in He for 1 h to remove any physisorbed molecules. Afterwards, the TPD experiment was started with a heating rate of 10 K min^{-1} under He flow (30 mL min^{-1}), and the desorbed CO_2 was monitored by a mass spectrometer (Pefeiffer Vacuum Quadstar, 32-bit).

2.3. Catalytic activity testing

Activity and selectivity measurements for CO_2 hydrogenation were carried out in a continuous flow, fixed-bed reactor. About 0.5 g of catalyst diluted with quartz sand (both in 40–60 mesh) was packed into the stainless steel tubular reactor (5 mm i.d.). Preliminary experiments with respect to possible influence caused by interparticle mass transfer limitation confirmed that such limitation could be ruled out under the conditions used in the present study. Prior to the catalytic measurements, the fresh catalyst was reduced in a stream of 10% H_2/N_2 flowing at 30 mL min^{-1} at 573 K for 3 h under atmospheric pressure. Then the reactor was cooled to a given temperature and a gas mixture (CO_2:H_2:N_2 = 22:66:12, molar ratio, GHSV = 2400 mL h^{-1} $g_{cat}{}^{-1}$) was introduced, raising the pressure to 3.0 MPa. All post reactor lines and valves were heated to 443 K to prevent possible product condensation. Effluent products were analyzed on-line with a gas chromatograph (6820, Agilent). Methanol was determined with a Porapak Q column, an FID detector and other gaseous products were determined with a Carbosieve column and a TCD detector. Conversion and selectivity values were calculated by mass-balance method, and the steady-state values were quoted as the average of seven different analyses taken after 4 h on stream operation.

3. Results and discussion

3.1. The structure of oxalate precursors

3.1.1. XRD analysis

Fig. 1 shows the XRD patterns of the dried precipitates prepared by oxalate co-precipitation method. Three main sharp diffraction peaks of the precipitates were observed at 2θ angles of 18.6°, 22.9° and 23.7°. These three peaks were identified as the diffraction lines of α-$ZnC_2O_4{\cdot}2H_2O$, $CuC_2O_4{\cdot}xH_2O$ and β-ZnC_2O_4, respectively [27]. After the addition of promoters to the CuO–ZnO catalyst, the diffraction peaks for α-$ZnC_2O_4{\cdot}2H_2O$ and $CuC_2O_4{\cdot}xH_2O$ weakened evidently and the line width broadened slightly. On the other hand, the diffraction peak for β-ZnC_2O_4 almost disappeared on the CZZ and CZTZ catalysts. This result indicates that a considerable amount of zinc was incorporated into the structure of $CuC_2O_4{\cdot}xH_2O$ by isomorphous substitution between copper and zinc after the addition of Zr [27,28]. From the XRD patterns of the Ti-containing samples (CZT and CZTZ), there is only a very weak diffraction peak of TiO_2 at 2θ angle of 27.4° due to the lower contents of Ti especially for the CZTZ catalyst. On the other hand, the weak diffraction peaks

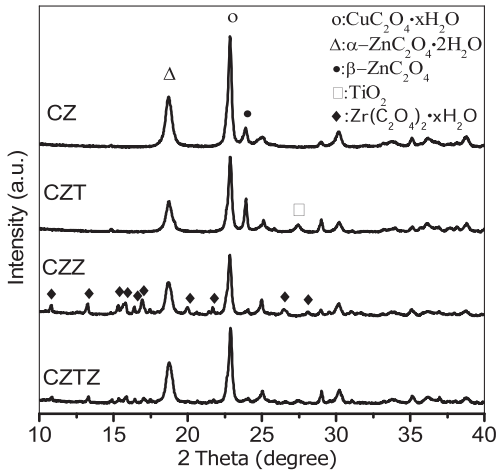

Fig. 1. XRD patterns for the oxalate precursors of different catalysts.

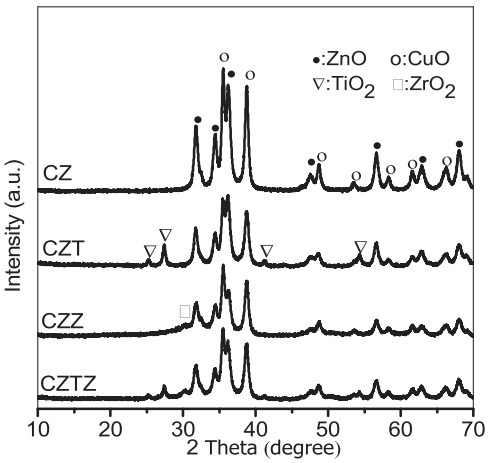

Fig. 3. XRD patterns of different catalysts.

observed at 2θ angles of 10.8°–17.4°, 20.0°, 21.7°, 26.5°, 28.1° for the samples of CZZ and CZTZ are identified as the diffraction lines of $Zr(C_2O_4)_2{\cdot}xH_2O$.

3.1.2. TG/DTG analyses

The TG/DTG patterns of the different oxalate precipitates are shown in Fig. 2. It indicates that the temperature for complete decomposition of the oxalate precipitates should be at ≥650 K (Fig. 2A). Based on these data, temperature of 673 K in ambient air was selected for the calcination process of all the samples in this work since calcination at even higher temperatures could result in increase in the crystallite size and decline in the surface area. On the other hand, as shown in Fig. 2B, three main peaks for the loss of weight are observed at about 383, 583, and 620 K for all the samples, and two extra peaks are observed at about 343 and 433 K for the samples with the addition of TiO_2 or ZrO_2. The peaks at about 343, 383, and 433 K (<473 K) can be due to the desorption of physically absorbed water and chemical structure water. The peaks at 583 and 620 K (denoted as α and β peaks, respectively) could be assigned to the decomposition of CuC_2O_4 and ZnC_2O_4 phases to form CuO and ZnO, respectively [27,28].

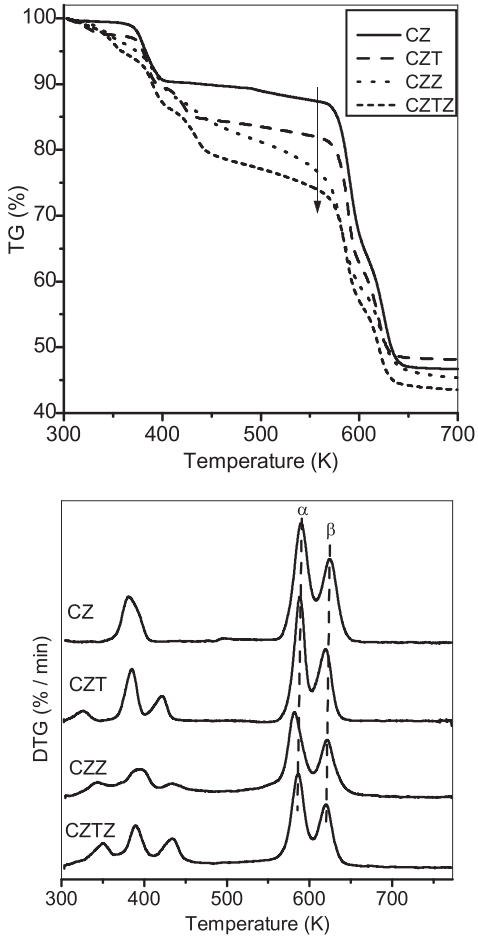

Fig. 2. TG (A) and DTG (B) patterns for the oxalate precursors of different catalysts.

3.2. Characterization of calcined catalysts

3.2.1. XRD and N_2 adsorption

Fig. 3 shows the XRD patterns of different catalysts after calcination at 673 K. The diffraction peaks at 35.6°, 38.8°, 48.8°, 53.7°, 58.3°, 61.6°, and 66.3° can be ascribed to the presence of CuO phase (PDF #48-1548), while the diffraction peaks at 31.8°, 34.4°, 36.3°, 47.7°, 56.7°, 62.9°, and 68.0° can be ascribed to the presence of ZnO phase (PDF #36-1451). The result indicates that the copper and zinc are present in the CuO and ZnO phases in the calcined catalysts, which is consistent with the TG/DTG results mentioned above. The only weak peak of ZrO_2 was at 30.3°, but the peaks of TiO_2 were at 25.3°, 27.5°, and 54.4°. As shown in Fig. 3, with the addition of TiO_2, ZrO_2, or TiO-ZrO_2, the intensity of peaks for CuO and ZnO weakened remarkably while the line width broadened slightly. This indicates that the crystallization degree of CuO and ZnO, as well as the particle sizes of CuO and ZnO crystallites (Table 1) decrease with the addition of TiO_2, ZrO_2, or TiO_2–ZrO_2, which leads to the larger S_{BET} and the smaller pore sizes (Table 1). On the other hand, the pore volumes of the catalysts have no obvious differences, as shown in Table 1.

3.2.2. AAS and XPS analyses

As shown in Table 2, the contents of Cu and Zn and Cu/Zn molar ratios of the calcined catalysts analyzed by AAS are in good line with those of the starting precursor salts added, indicating that the composition of the CuO–ZnO-based catalysts prepared by the oxalate co-precipitation method can be precisely controlled.

Fig. 4 shows the XPS patterns of the Cu 2p, Zn 2p, Ti 2p, and Zr 3d for the four catalysts. The binding energies (BE) of Cu $2p_{3/2}$, $Zn3d_{3/2}$, $Ti2p_{3/2}$, and Zr $3d_{5/2}$ core electrons are summarized in Table 3. The $Cu2p_{3/2}$ and $Cu2p_{1/2}$ peaks (Fig. 4A) appeared at around 933 and 953 eV, which are characteristic of Cu^{2+} species [29]. An

Table 1
Physicochemical properties of the different catalysts.

Catalyst	S_{BET} (m^2/g)	Pore size (nm)	Pore volume (cm^3/g)	D^a_{CuO} (nm)	D^a_{ZnO} (nm)	S_{Cu} (m^2/g)
CZ	26.3	27.7	0.18	18.9	15.1	4.89
CZT	37.3	22.2	0.21	16.4	14.9	5.17
CZZ	39.1	18.9	0.18	17.0	14.3	6.62
CZTZ	38.7	19.5	0.19	15.8	14.1	9.21

[a] The crystallite size was estimated by Scherrer's equation.

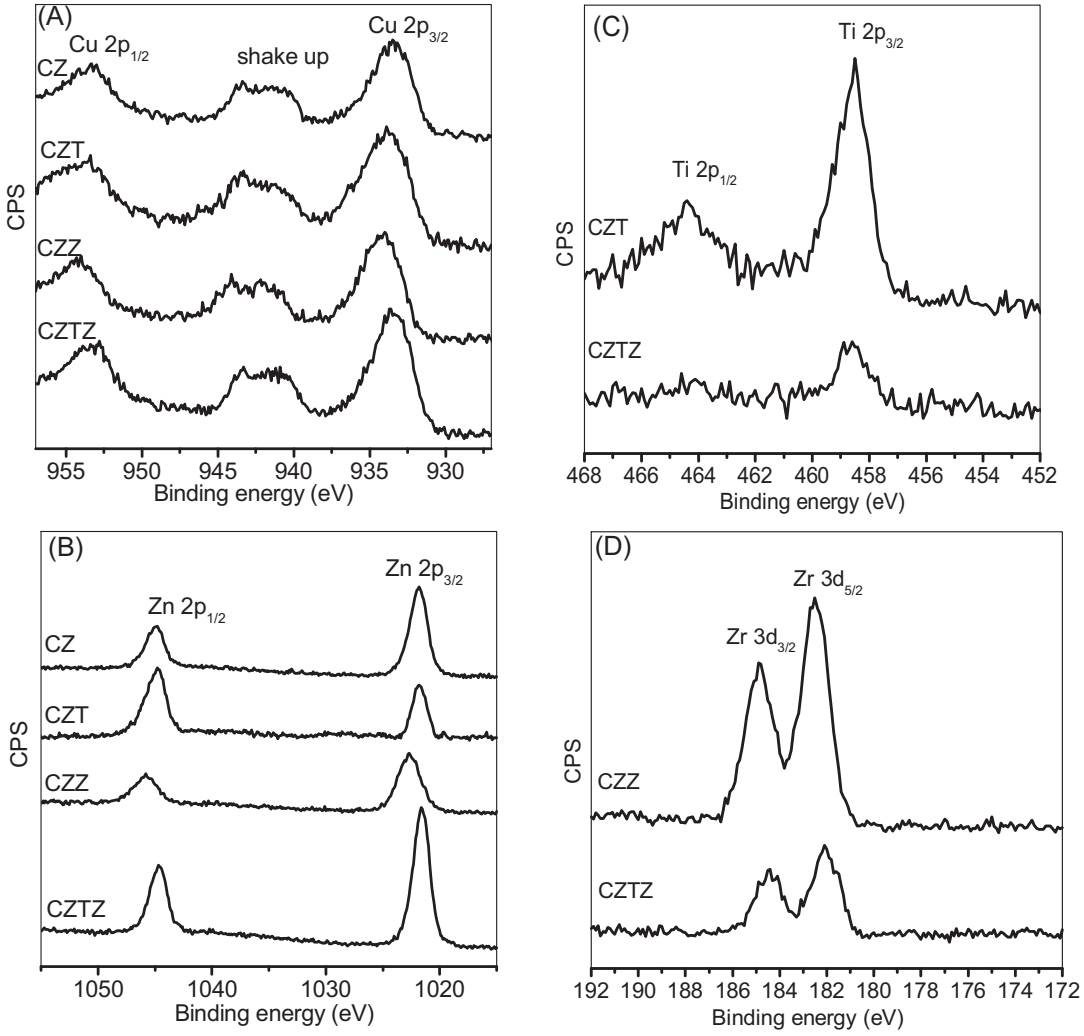

Fig. 4. XPS patterns of different catalysts: (A) Cu, (B) Zn, (C) Ti, and (D) Zr.

additional means of identifying Cu^{2+} is the satellite peaks between 940 and 945 eV, which are caused by electron shake-up process [30]. It indicates that copper species are present as Cu^{2+} in all calcined catalysts. The binding energy of the $Zn2p_{3/2}$ peak (Fig. 4B) at around 1022 eV indicates that Zn is present as ZnO [31]. The data of the Ti $2p_{3/2}$ and Ti $2p_{1/2}$ binding energy of the CZT and CZTZ samples are in good agreement with the reported values for Ti^{4+} in anatase TiO_2 [14]. The values of $Zr3d_{5/2}$ binding energy of the CZZ and CZTZ catalysts reveal that zirconium species exist in the form of ZrO_2 [32]. The above results reveal that the chemical states of Cu and Zn are not influenced noticeably by the addition of TiO_2 or ZrO_2.

Table 2
Contents of Cu and Zn and Cu/Zn molar ratio of the calcined catalysts.

Catalyst	Content (at.%)[a,b]				Cu/Zn molar ratio[a]
	Cu	Zn	Ti	Zr	
CZ	49.5 (50)	50.5 (50)	–	–	0.98 (1)
CZT	41.2(40)	45.5 (40)	nd (20)	–	0.91 (1)
CZZ	40.1 (40)	36.6 (40)	–	nd (20)	1.09 (1)
CZTZ	41.0 (40)	41.3 (40)	nd (10)	nd (10)	0.99 (1)

[a] Values in parenthesis are nominal fractions of metals.
[b] nd: not determined.

Surface compositions of the catalysts determined with the XPS method are also listed in Table 3. Compared with the average compositions in the bulk catalysts (as seen in Table 2), the surface of catalysts are considerably depleted of Cu. In contrast, an enrichment of Zn on the surface is observed. Similar results were also reported by some researchers on other Cu-ZnO-based catalysts [33,34]. Moreover, the surface Cu/Zn ratios of the catalysts are also included in Table 3. Clearly, the surface Cu/Zn

Table 3
XPS results for the different catalysts.

Catalyst	Binding energy (eV)				Relative surface concentration of metal (at.%)				Cu/Zn molar ratio
	Cu $2p_{3/2}$	Zn $2p_{3/2}$	Ti $2p_{3/2}$	Zr $3d_{5/2}$	Cu	Zn	Ti	Zr	
CZ	933.5	1021.8	–	–	48.2	51.8	0	0	0.93
CZT	933.9	1022.5	458.5	–	36.2	51.7	12.1	0	0.70
CZZ	934.0	1021.7	–	182.5	32.0	36.1	0	31.9	0.89
CZTZ	933.6	1021.6	458.6	182.1	38.1	47.3	4.9	9.7	0.81

ratios of the modified CuO–ZnO catalysts are much lower than the bulk one (Table 2). On the other hand, comparing with the data as seen in Table 2, the relative surface concentration of TiO_2 is lower than nominal fraction for the CZT and CZTZ catalysts. However, the relative surface concentration of ZrO_2 is much higher than the nominal fraction for the CZZ catalyst, indicating that the surface of CuO is covered partly by ZrO_2 on the CZZ catalyst.

3.2.3. TPR analysis

To investigate the reduction behavior of the catalysts, TPR measurements were carried out and the results are shown in Fig. 5. There is only one broad reduction peak in the TPR profiles of the four catalysts, and the temperature of the peak occurs in the range of 438–527 K. Since ZnO, TiO_2, and ZrO_2 are not reduced within the experimental regions, the reduction peaks are related to the reduction of CuO species. The peaks shifted from 486 K for CuO–ZnO to a higher temperature of 492 K for CuO–ZnO–TiO_2, while to lower temperatures of 483 and 477 K for CuO–ZnO–ZrO_2 and CuO–ZnO–TiO_2–ZrO_2, respectively. The TPR analysis shows that the reduction temperature of the catalysts is in an order of CZT > CZ > CZZ > CZTZ. Interestingly, as observed by XRD analysis (Fig. 3 and Table 1), the crystallite sizes of CuO present in the catalysts are in an order of CZTZ < CZT < CZZ < CZ. It indicates that the addition of ZrO_2 can enhance the dispersion of CuO and decrease the crystallite sizes of CuO, leading to the easier reduction of CuO. However, the added TiO_2 can increase the interaction between CuO and ZnO or TiO_2, resulting in higher reduction temperature. On the other hand, compared with the catalyst CuO–ZnO, the reduction peak areas of the modified CuO–ZnO catalysts decrease due to the decline in the content of Cu in the catalysts (Table 2).

3.3. Characterization of the reduced catalysts

3.3.1. S_{Cu} measurement

The S_{Cu} values of the reduced Cu–ZnO catalysts before and after modification with TiO_2, ZrO_2, or TiO_2–ZrO_2 are presented in Table 1. It can be seen that although the CuO contents of the modified catalysts are lower than that of the catalyst CuO–ZnO, the S_{Cu} values increased after modification, which can be attributed to the enhanced dispersion of CuO as evidenced by XRD results (Fig. 3). The S_{Cu} values increase in the order of CZ < CZT < CZZ < CZTZ, and the S_{Cu} value of CZTZ sample (9.21 m^2/g) is almost twice the large of CZ sample (4.89 m^2/g). A similar result was also obtained previously for the CuO–TiO_2–ZrO_2 catalysts with different CuO contents (50–80%): the S_{Cu} of the catalyst with 70% CuO (7.94 m^2/g) was almost two times higher than that of the catalyst with 80% CuO (4.16 m^2/g) [35].

3.3.2. H_2-TPD

The H_2-TPD profiles for the pre-reduced catalysts are presented in Fig. 6. As seen, all the patterns span a wide range of temperature (323–773 K). Two desorption peaks can be observed for all the investigated catalysts, which is diagnostic of different adsorption states of hydrogen species across the catalyst structure. According to literature data, only the resolved peak at low temperature is ascribable to atomic hydrogen on surface Cu sites, while a large signal at high temperature monitors the desorption of hydrogen from either the bulk of Cu particles or ZnO surface [36,37]. As seen from Fig. 6, with the addition of promoters, the α and β peaks shift to higher temperatures slightly, from 349 and 661 K to 369 and 669 K, respectively. The quantitative data of H_2 desorbed over different catalysts are listed in Table 4. It was found that the amount of H_2 desorbed from Cu sites increases in the order of CZ < CZT < CZZ < CZTZ, which is in accordance with the variation of S_{Cu} (Table 1). However, the amounts of hydrogen desorbed from either the bulk of Cu particles or ZnO surface on different catalyst

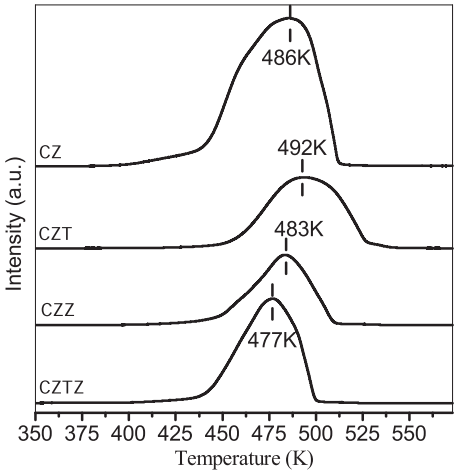

Fig. 5. H_2-TPR patterns of different catalysts.

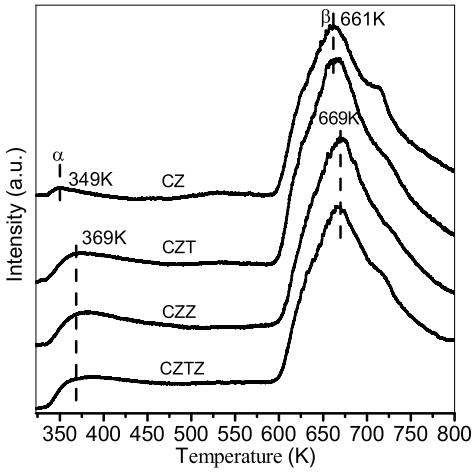

Fig. 6. H_2-TPD patterns of different catalysts after reduction.

Table 4
The amounts of H_2 and CO_2 adsorbed over different catalysts.

Catalyst	Amount of H_2 adsorbed		Amount of CO_2 adsorbed	
	A_α (a.u.)	A_β (a.u.)	A_α (a.u.)	A_β (a.u.)
CZ	7	256	15	19
CZT	33	305	37	9
CZZ	38	267	55	18
CZTZ	45	246	94	16

are very similar except for CZT with the largest value (Table 4). On the other hand, it should be emphasized that only the H_2 desorbed at lower temperature is useful for the synthesis of methanol from CO_2 hydrogenation since the reaction usually takes place below 623 K [37].

3.3.3. CO_2-TPD

Fig. 7 shows the CO_2-TPD curves of the reduced Cu–ZnO catalysts before and after modification with TiO_2, ZrO_2, or TiO_2–ZrO_2. Two desorption peaks (denoted as α and β, respectively) are observed in lower and higher temperature ranges, corresponding to CO_2 desorbed from a weak basic site and a strong basic site, respectively. As can be noted, the shift of α peak from 392 to 387 K indicates that the weak basic site becomes weaker with the addition of promoters, while the temperature of β peak (650 K) has no noticeable change, indicating that the addition of promoters has no noticeable effect on the strength of the strong basic site. The quantitative data of CO_2 desorbed over different catalysts are also listed in Table 4. It can be seen that the amount of weak basic site over the modified Cu–ZnO catalysts is larger than that over the parent Cu–ZnO catalyst and increases in the order of CZ < CZT < CZZ < CZTZ, indicating that the addition of TiO_2 and ZrO_2 improves the amount of weak basic site and the TiO_2–ZrO_2 binary oxide exhibits greater effect than the single oxides of TiO_2 and ZrO_2. This result is in line with those reported in the literature [38,39] that the amount of basic site of TiO_2–ZrO_2 was larger than those of TiO_2 and ZrO_2. However, the amounts of strong basic sites on different catalyst are very similar except for CZT with the smallest value (Table 4). On the other hand, considering the reaction temperature used in the present work (≤553 K), the CO_2 desorbed from low temperature seems to be rather related with the active site for methanol synthesis from CO_2 hydrogenation than that from high temperature at around 650 K, which is much higher than the actual reaction temperature. That means that the CO_2 adsorbed on those sites is rather difficult to desorb under reaction conditions and might not take part in the reaction [40].

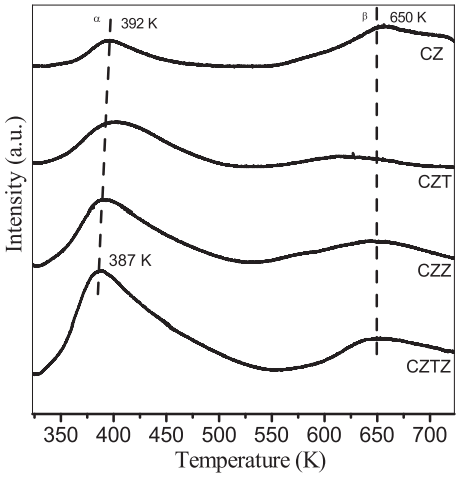

Fig. 7. CO_2-TPD patterns of different catalysts after reduction.

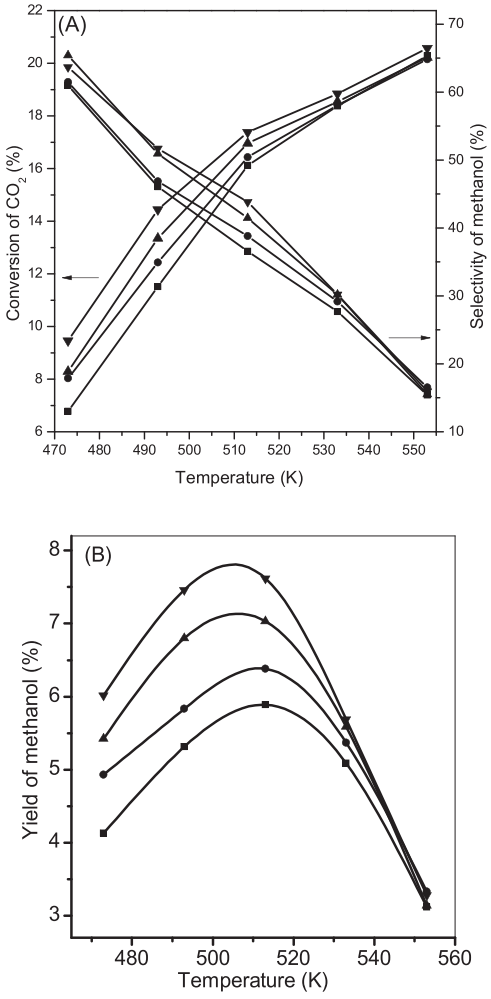

Fig. 8. Effect of reaction temperature on the conversion of CO_2, the selectivity of methanol (A) and the yield of methanol (B) over the different catalysts. (■) CZ; (●) CZT; (▲) CZZ; (▼) CZTZ. Reaction conditions: H_2/CO_2 = 3 (v/v), P = 3.0 MPa, GHSV = 2400 mL h^{-1} g_{cat}^{-1}.

3.4. Catalytic performance

Activity and selectivity measurement results for methanol synthesis from CO_2 hydrogenation over the different catalysts are summarized in Fig. 8. Methanol and CO are the only carbon-containing products under the present reaction conditions. The effect of reaction temperature on the catalytic performance of Cu–ZnO-based catalysts with different promoters was investigated. As seen from Fig. 8A, for all the catalysts, the conversion of CO_2 increased with the increase in reaction temperature, accompanied by a decrease in methanol selectivity, over the temperature range of 473–553 K. The variation of methanol yield with reaction temperature is presented in Fig. 8B. Clearly, a maximum yield of methanol, which represents the critical point of the reaction transforming from kinetics to thermodynamics, exists for all the catalysts studied [28]. Furthermore, it is clear that the addition of promoter is favorable for the production of methanol and the sample of CZTZ shows the highest methanol yield, as shown in Fig. 8B.

It is worth noting that the differences in the CO_2 conversion between the parent and modified Cu–ZnO catalysts decrease with an increase in the reaction temperature (Fig. 8A), because the CO_2 conversion is approaching the equilibrium conversion. Therefore, the activity comparison between the different catalysts would be meaningful at the low reaction temperatures. From this point of view, the CO_2 conversion, methanol selectivity, and yield over the

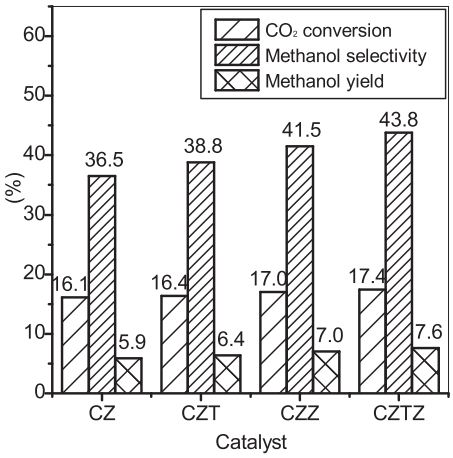

Fig. 9. Effect of different promoters on catalytic performance of Cu–ZnO-based catalysts. Reaction conditions: $T = 513$ K, $H_2/CO_2 = 3$ (v/v), $P = 3.0$ MPa, GHSV = 2400 mL h^{-1} g_{cat}^{-1}.

different catalysts at 513 K are presented in Fig. 9. As shown in Fig. 9, the conversion of CO_2 increases with the addition of promoters and a maximum of 17.4% is observed over the sample of CZTZ. The value of CH_3OH selectivity is 43.8% over the same sample (CZTZ), which is 20% higher than that on the CZ catalyst. The highest yield of CH_3OH was obtained over the CZTZ catalyst, and the value increased by about 30% (from 5.9 to 7.6%) in comparison with the parent CZ catalyst. These results indicate that the promoters of TiO_2 and ZrO_2 can enhance the hydrogenation activity of the Cu–ZnO catalysts and the TiO_2–ZrO_2 mixed oxide is the best.

For the Cu-based catalyst, Fisher and Bell [41] proposed that there are two active centers involved in the catalytic process of CO_2 hydrogenation. One is the so-called "support" and it serves to adsorb CO_2 as carbonate and bicarbonate species which could undergo stepwise hydrogenation to methanol. The other is the Cu component, and it serves to adsorb H_2 dissociatively and to provide atomic hydrogen to the surface of support by spillover. The proposed mechanism and the role of hydrogen spillover from Cu to support were supported by H_2/D_2 isotopic tracer studies [42]. Such a mechanism is known as "dual-site" mechanism, and it has been accepted currently by many researchers [21,24,43,44]. Accordingly, it is reasonable to consider the S_{Cu} and the adsorption property of

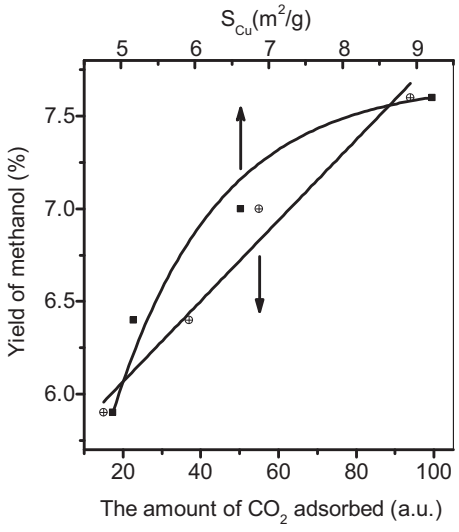

Fig. 10. The relationships between the yield of methanol and the amount of adsorbed CO_2 (□) and S_{Cu} (■).

CO_2 with contribution to the methanol synthesis at the same time. Therefore, the effects of the S_{Cu} and the amounts of adsorbed CO_2 on the activity of methanol synthesis from CO_2 hydrogenation over the Cu–ZnO-based catalysts with different promoters were studied and the results are shown in Fig. 10. It can be seen that the yield of methanol increases with the increase in the S_{Cu}, but it is not a linear relationship. However, the yield of methanol increases linearly with increasing the amounts of adsorbed CO_2 of the catalysts. Thus, we can deduce that the values of S_{Cu} for these catalysts are relatively large, but the amounts of adsorbed CO_2 are insufficient. That is to say, the catalytic activity for methanol synthesis mainly depends on the amount of adsorbed CO_2 rather than the S_{Cu} for these catalysts in the present study. This observation also suggests that the full benefit of the increased S_{Cu} is not achieved because the CO_2 adsorption limits the methanol synthesis activity of the catalysts.

4. Conclusions

CuO–ZnO-based catalysts with various promoters (TiO_2, ZrO_2, or TiO_2–ZrO_2 mixed oxide) were prepared via oxalate co-precipitation method for methanol synthesis from CO_2 hydrogenation. The influences of promoters on the physicochemical and catalytic properties for methanol synthesis from CO_2 hydrogenation of the CuO–ZnO catalysts were investigated. Based on the results of this paper, the following conclusions can be made:

(1) The CO_2 conversion and methanol yield increase with the addition of promoters, and their maxima are obtained over the TiO_2–ZrO_2 mixed oxide modified CuO–ZnO catalyst.
(2) The addition of TiO_2, ZrO_2, or TiO_2–ZrO_2 leads to a decrease in crystallite sizes of CuO and ZnO, and enlarges the metallic copper surface area of the CuO–ZnO catalyst.
(3) The amounts of basic sites and H_2 adsorption increase with the addition of TiO_2, ZrO_2, or TiO_2–ZrO_2, and the TiO_2–ZrO_2 mixed oxide modified CuO–ZnO catalyst has the maximum amounts of basic sites and H_2 adsorption.
(4) The linear relationship between the yield of methanol and the CO_2 adsorption capacity of the catalysts substantiates the dual-site mechanism of the methanol synthesis from CO_2 hydrogenation.

Acknowledgements

The authors thank Shanghai Municipal Education Commission (13YZ117) and Science and Technology Commission of Shanghai Municipality (13ZR1441200) for financial supports.

References

[1] L. Barbato, G. Centi, G. Iaquaniello, A. Mangiapane, S. Perathoner, Trading renewable energy by using CO_2: an effective option to mitigate climate change and increase the use of renewable energy sources, Energy Technol. 2 (2014) 453–461.
[2] E.V. Kondratenko, G. Mul, J. Baltrusaitis, G.O. Larrazábal, J. Pérez-Ramírez, Status and perspectives of CO_2 conversion into fuels and chemicals by catalytic, photocatalytic and electrocatalytic processes, Energy Environ. Sci. 6 (2013) 3112–3135.
[3] G. Centi, E.A. Quadrelli, S. Perathoner, Catalysis for CO_2 conversion: a key technology for rapid introduction of renewable energy in the value chain of chemicals industries, Energy Environ. Sci. 6 (2013) 1711–1731.
[4] F. Pontzen, W. Liebner, V. Gronemann, M. Rothaemel, B. Ahlers, CO_2-based methanol and DME-Efficient technologies for industrial scale production, Catal. Today 171 (2011) 242–250.
[5] F.L. Liao, Z.Y. Zeng, C. Eley, Q. Lu, X.L. Hong, S.C.E. Tsang, Electronic modulation of a copper/zinc oxide catalyst by a heterojunction for selective hydrogenation of carbon dioxide to methanol, Angew. Chem. Int. Ed. 51 (2012) 5832–5836.
[6] G.A. Olah, Towards oil independence through renewable methanol chemistry, Angew. Chem. Int. Ed. 52 (2013) 104–107.

[7] F. Arena, G. Italiano, K. Barbera, S. Bordiga, G. Bonura, L. Spadaro, F. Frusteri, Solid-state interactions, adsorption sites and functionality of Cu–ZnO/ZrO_2 catalysts in the CO_2 hydrogenation to CH_3OH, Appl. Catal. A 350 (2008) 16–23.
[8] S. Natesakhawat, J.W. Lekse, J.P. Baltrus, P.R. Ohodnicki Jr., B.H. Howard, X.Y. Deng, C. Matranga, Active sites and structure–activity relationships of copper-based catalysts for carbon dioxide hydrogenation to methanol, ACS Catal. 2 (2012) 1667–1676.
[9] G.J.J. Bartley, R. Burch, Support and morphological effects in the synthesis of methanol over Cu/ZnO, Cu/ZrO_2 and Cu/SiO_2 catalysts, Appl. Catal. 43 (1988) 141–153.
[10] Y. Zhang, J. Fei, Y. Yu, X. Zheng, Methanol synthesis from CO_2 hydrogenation over Cu based catalyst supported on zirconia modified gamma-Al_2O_3, Energy Convers. Manage. 47 (2006) 3360–3367.
[11] K.K. Bando, K. Sayama, H. Kusama, K. Okabe, H. Arakawa, In-situ FT-IR study on CO_2 hydrogenation over Cu catalysts supported on SiO_2, $A1_2O_3$, and TiO_2, Appl. Catal. A 165 (1997) 391–409.
[12] J. Xiao, D.S. Mao, X.M. Guo, J. Yu, Methanol synthesis from CO_2 hydrogenation over CuO–ZnO–TiO_2 catalysts: the influence of TiO_2 content, Energy Technol. 3 (2015) 32–39.
[13] T. Tagawa, N. Nomur, M. Shimakage, S. Goto, Effect of supports on copper catalysts for methanol synthesis from $CO_2 + H_2$, Res. Chem. Intermed. 21 (1995) 193–202.
[14] H. Arakawa, K. Sayama, K. Okabe, A. Murakami, Promoting effect of TiO_2 addition to CuO–ZnO catalyst on methanol synthesis by catalytic hydrogenation of CO_2, Stud. Surf. Sci. Catal. 77 (1993) 389–392.
[15] T.C. Schilke, I.A. Fisher, A.T. Bell, In situ infrared study of methanol synthesis from CO_2/H_2 on titania and zirconia promoted Cu/SiO_2, J. Catal. 184 (1999) 144–156.
[16] M. Saito, T. Fujitani, M. Takeuchi, T. Watanabe, Development of copper/zinc oxide-based multicomponent catalysts for methanol synthesis from carbon dioxide and hydrogen, Appl. Catal. A 238 (1996) 311–318.
[17] N. Nomura, T. Tagawa, S. Goto, In situ FTIR study on hydrogenation of carbon dioxide over titania-supported copper catalyst, Appl. Catal. A 166 (1998) 321–326.
[18] X.M. Guo, D.S. Mao, G.Z. Lu, S. Wang, G.S. Wu, Glycine-nitrate combustion synthesis of CuO–ZnO–ZrO_2 catalysts for methanol synthesis from CO_2 hydrogenation, J. Catal. 271 (2010) 178–185.
[19] L. Li, D.S. Mao, J. Yu, X.M. Guo, Highly selective hydrogenation of CO_2 to methanol over CuO–ZnO–ZrO_2 catalysts prepared by a surfactant-assisted coprecipitation method, J. Power Sources 279 (2015) 394–404.
[20] F. Arena, G. Mezzatesta, G. Zafarana, G. Trunfio, F. Frusteri, L. Spadaro, Effects of oxide carriers on surface functionality and process performance of the Cu–ZnO system in the synthesis of methanol via CO_2 hydrogenation, J. Catal. 300 (2013) 141–151.
[21] G. Bonura, F. Arena, G. Mezzatesta, C. Cannilla, L. Spadaro, F. Frusteri, Role of the ceria promoter and carrier on the functionality of Cu-based catalysts in the CO_2-to-methanol hydrogenation reaction, Catal. Today 171 (2011) 251–256.
[22] L.X. Zhang, Y.C. Zhang, S.Y. Chen, Effect of promoter SiO_2, TiO_2 or SiO_2–TiO_2 on the performance of CuO–ZnO–Al_2O_3 catalyst for methanol synthesis from CO_2 hydrogenation, Appl. Catal. A 415–416 (2012) 118–123.
[23] Y. Nitta, O. Suwata, Y. Ikeda, Y. Okamoto, T. Imanaka, Copper–zirconia catalysts for methanol synthesis from carbon dioxide: effect of ZnO addition to Cu–ZrO_2 catalysts, Catal. Lett. 26 (1994) 345–354.
[24] X.M. Guo, D.S. Mao, G.Z. Lu, S. Wang, G.S. Wu, The influence of La doping on the catalytic behavior of Cu/ZrO_2 for methanol synthesis from CO_2 hydrogenation, J. Mol. Catal. A 345 (2011) 60–68.
[25] N. Nomura, T. Tagawa, S. Goto, Effect of acid–base properties on copper catalysts for hydrogenation of carbon dioxide, React. Kinet. Catal. Lett. 63 (1998) 21–25.
[26] Y.P. Zhao, L.H. Jia, T. Jing, D.Z. Sun, J.S. Chung, Effect of ZrO_2 on the performance of CuO–ZnO–TiO_2–ZrO_2 catalysts used in methanol synthesis from CO_2 hydrogenation, Asian J. Chem. 24 (2012) 2245–2248.
[27] Y. Ma, Q. Sun, D. Wu, W.H. Fan, Y.L. Zhang, J.F. Deng, A practical approach for the preparation of high activity Cu/ZnO/ZrO_2 catalyst for methanol synthesis from CO_2 hydrogenation, Appl. Catal. A 171 (1998) 45–55.
[28] Q. Sun, Y.L. Zhang, H.Y. Chen, J.F. Deng, D. Wu, S.Y. Chen, A novel process for the preparation of Cu/ZnO and Cu/ZnO/Al_2O_3 ultrafine catalyst: structure, surface properties, and activity for methanol synthesis from $CO_2 + H_2$, J. Catal. 167 (1997) 92–105.
[29] R.T. Figueiredo, A. Martínez-Arias, M.L. Granados, J.L.G. Fierro, Spectroscopic evidence of Cu–Al interactions in Cu–Zn–Al mixed oxide catalysts used in CO hydrogenation, J. Catal. 178 (1998) 146–152.
[30] J. Toyir, P. Ramírez de la Piscina, J.L.G. Fierro, N. Homs, Highly effective conversion of CO_2 to methanol over supported and promoted copper-based catalysts: influence of support and promoter, Appl. Catal. B 29 (2001) 207–215.
[31] S. Velu, K. Suzuki, C.S. Gopinath, H. Yoshida, T. Hattori, X.P.S. XANES, EXAFS investigations of CuO/ZnO/Al_2O_3/ZrO_2 mixed oxide catalysts, Phys. Chem. Chem. Phys. 4 (2002) 1990–1999.
[32] K. Sun, W. Lu, F. Qiu, S. Liu, X. Xu, Direct synthesis of DME over bifunctional catalyst: surface properties and catalytic performance, Appl. Catal. A 252 (2003) 243–249.
[33] W.L. Dai, Q. Sun, J.F. Deng, D. Wu, Y.H. Sun, XPS studies of Cu/ZnO/Al_2O_3 ultrafine catalysts derived by a novel gel oxalate co-precipitation for methanol synthesis by $CO_2 + H_2$, Appl. Surf. Sci. 177 (2001) 172–179.
[34] J. Sloczynski, R. Grabowski, P. Olszewski, A. Kozlowska, J. Stoch, M. Lachowska, J. Skrzypek, Effect of metal oxide additives on the activity and stability of Cu/ZnO/ZrO_2 catalysts in the synthesis of methanol from CO_2 and H_2, Appl. Catal. A 310 (2006) 127–137.
[35] S. Wang, D.S. Mao, X.M. Guo, G.Z. Lu, Dimethyl ether synthesis from CO_2 hydrogenation over CuO–TiO_2–ZrO_2/HZSM-5 catalysts, Acta Phys. Chim. Sin. 27 (2011) 2651–2658.
[36] P. Gao, F. Li, N. Zhao, F. Xiao, W. Wei, L.S. Zhong, Y.H. Sun, Influence of modifier (Mn, La, Ce, Zr and Y) on the performance of Cu/Zn/Al catalysts via hydrotalcite-like precursors for CO_2 hydrogenation to methanol, Appl. Catal. A 468 (2013) 442–452.
[37] H.J. Zhan, F. Li, P. Gao, N. Zhao, F.K. Xiao, W. Wei, L.S. Zhong, Y.H. Sun, Methanol synthesis from CO_2 hydrogenation over La–M–Cu–Zn–O (M = Y, Ce, Mg, Zr) catalysts derived from perovskite-type precursors, J. Power Sources 251 (2014) 113–121.
[38] K. Arata, H. Sawamura, The dehydration and dehydrogenation of ethanol catalyzed by TiO_2–ZrO_2, Bull. Chem. Soc. Jpn. 48 (1975) 3377–3378.
[39] K. Hashimoto, T. Masuda, H. Kashihara, Effects of acidic and basic properties on selectivity in the reforming of *n*-hexane over a binary oxide of titanium and zirconium supporting a platinum catalyst, Appl. Catal. 75 (1991) 331–342.
[40] K.W. Jun, W.J. Shen, K.S. Rama Rao, K.W. Lee, Residual sodium effect on the catalytic activity of Cu/ZnO/Al_2O_3 in methanol synthesis from CO_2 hydrogenation, Appl. Catal. A 174 (1998) 231–238.
[41] I.A. Fisher, A.T. Bell, In-situ infrared study of methanol synthesis from H_2/CO_2 over Cu/SiO_2 and Cu/ZrO_2/SiO_2, J. Catal. 172 (1997) 222–237.
[42] K.D. Jung, A.T. Bell, Role of hydrogen spillover in methanol synthesis over Cu/ZrO_2, J. Catal. 193 (2000) 207–223.
[43] F. Arena, G. Mezzatesta, G. Zafaana, G. Trunfio, F. Frusteri, L. Spadaro, How oxide carriers control the catalytic functionality of Cu–ZnO system in the hydrogenation of CO_2 to methanol, Catal. Today 210 (2013) 39–46.
[44] P. Gao, F. Li, H.J. Zhang, N. Zhao, F. Xiao, W. Wei, L.S. Zhong, Y.H. Sun, Fluorine-modified Cu/Zn/Al/Zr catalysts via hydrotalcite-like precursors for CO_2 hydrogenation to methanol, Catal. Commun. 50 (2014) 78–82.